

FLARE ACTIVITY AND MAGNETIC HELICITY INJECTION BY PHOTOSPHERIC HORIZONTAL MOTIONS

Y.-J. MOON^{1,2}, JONGCHUL CHAE^{1,3}, G. S. CHOE⁴, HAIMIN WANG¹, Y. D. PARK²,
H. S. YUN⁵, VASYL YURCHYSHYN¹, AND PHILIP R. GOODE¹

ABSTRACT

We present observational evidence that the occurrence of homologous flares in an active region is physically related to the injection of magnetic helicity by horizontal photospheric motions. We have analyzed a set of 1 minute cadence magnetograms of NOAA AR 8100 taken over a period of 6.5 hours by Michelson Doppler Imager (MDI) on board Solar and Heliospheric Observatory (SOHO). During this observing time span, seven homologous flares took place in the active region. We have computed the magnetic helicity injection rate into the solar atmosphere by photospheric shearing motions, and found that a significant amount of magnetic helicity was injected during the observing period. In a strong M4.1 flare, the magnetic helicity injection rate impulsively increased and peaked at the same time as the X-ray flux did. The flare X-ray flux integrated over the X-ray emission time strongly correlates with the magnetic helicity injected during the flaring interval. The integrated X-ray flux is found to be a logarithmically increasing function of the injected magnetic helicity. Our results suggest that injection of helicity and abrupt increase of helicity magnitude play a significant role in flare triggering.

Subject headings: Sun: magnetic fields — Sun: flare — Sun: photosphere

¹Big Bear Solar Observatory, NJIT, 40386 North Shore Lane, Big Bear City, CA 92314 (yj-moon@bbso.njit.edu)

²Korea Astronomy Observatory, Whaamdong, Yooseong-ku, Daejeon, 305-348, Korea

³Department of Astronomy and Space Science, Chungnam National University, Daejeon 305-764, Korea

⁴Plasma Physics Laboratory, Princeton University, Princeton, NJ 08543-0451, USA

⁵Astronomy Program, SEES, Seoul National University, Seoul 151-742, Korea

1. INTRODUCTION

There have been many reports on the helical structure of solar and heliospheric magnetic fields as observed in photospheric magnetic fields (Pevtsov & Canfield 1999), coronal X-ray images (Canfield & Pevtsov 1999), solar filaments (Chae 2000), coronal mass ejections (Rust 1999), and interplanetary magnetic fields (Burlaga 1988). So far most observational studies of the helicity in solar active regions have focused on the current helicity, defined as $\int \mathbf{B} \cdot \mathbf{J} dV$, and its sign (or the linear force-free coefficient α), mainly because they can be directly inferred from photospheric vector magnetograms (e.g., Hagyard & Pevtsov 1999). The current helicity is a measure of the topological properties such as twist and mutual linkages of the lines of electric current (Berger & Field 1984; DeVore 2000). On the other hand, magnetic helicity, defined as $\int \mathbf{A} \cdot \mathbf{B} dV$, is a measure of twist and linkage of magnetic field lines (DeVore 2000). The magnetic helicity is a physically more useful concept than the current helicity, because magnetic helicity is fairly well-conserved in a closed volume, whose boundary is not crossed by any field lines, as well as in an open volume, in which a boundary normal flux exists, in the absence of boundary flows (e.g., Berger & Field 1984). It is considered as a robust invariant in space plasmas such as the solar corona (Berger 1999). However, the magnetic helicity has rarely been measured because of the difficulty in determining the topological connection of field lines in a 3D space. Instead, there have been efforts to determine its rate in an open volume.

Since the solar corona is an open volume with the photosphere as a boundary with normal flux, the magnetic helicity can be transported across the boundary by velocity fields in the photosphere. According to Berger & Field (1984), the Poynting theorem for magnetic helicity in an open volume is given by

$$\frac{dH}{dt} = 2 \oint (\mathbf{B} \cdot \mathbf{A}_p) v_z dS - 2 \oint (\mathbf{v} \cdot \mathbf{A}_p) B_z dS, \quad (1)$$

where \mathbf{A}_p is the unique vector potential of the potential field satisfying the following conditions:

$$\nabla \times \mathbf{A}_p \cdot \mathbf{z} = B_z, \quad \nabla \cdot \mathbf{A}_p = 0, \quad \mathbf{A}_p \cdot \mathbf{z} = 0. \quad (2)$$

Equation (1) tells that the magnetic helicity in an open volume can change either by the passage of field lines through the surface (first term, which is called advection term) or by the horizontal motions of field lines (second term or shear term). Recently, Chae (2001) developed a direct method of deriving the shear term from observations. In this paper, we apply this methodology to a set of MDI (Scherrer et al. 1995) 1-min full-disk longitudinal magnetograms of NOAA AR 8100, where several homologous flares took place. We are specifically interested in revealing any probable relationship between GOES X-ray fluxes of individual flares and magnetic helicity changes caused by photospheric horizontal motions.

Kusano et al. (2002) also studied the helicity injection rate in the same active region for several days using 96-min MDI data. However, they could not examine one-to-one correspondence between individual flaring activity and helicity injection rate because of the limitation in time resolution. Since we determine only the shear term in Equation (1), there may be a worry that it is not possible to determine dH/dt unless the advection term is negligible. However, as it will be shown later, no significant amount of flux emergence was found during our observing period. This may imply that the advection term is insignificant and the shear term dominates dH/dt , at least, during our observing period.

Generally, homologous flares occur repeatedly in an active region, at the nearly same position, with a common pattern of development. Since they are thought to experience a similar physical process of energy storage and release, it is physically meaningful to examine the relationship between helicity change and X-ray flux in a set of homologous flares. There are a few mechanisms proposed for homologous flares. Ranns et al. (2000) made multi-wavelength observations of two M class flares and suggested a schematic reconnection scenario for two loops interaction with emerging fluxes. From a variety of space and ground-based observations Woodgate et al. (1984) reported that most homologous flares have strong horizontal photospheric flows together with high magnetic shear. On this basis, Choe & Cheng (2000) demonstrated using resistive MHD simulations, that a series of homologous flares can be induced by continuing shearing motions.

Our results strongly indicate that photospheric shearing motions did play an important role in generating the homologous flares that occurred in NOAA AR 8100.

2. DATA AND ANALYSIS

We have used a set of MDI 1 minute full-disk longitudinal magnetograms, which were obtained from 21:32 UT on November 3 to 4:00 UT on November 4, 1997. The full disk magnetograms were recorded by a 1024×1024 CCD detector with a pixel size of $2''$. The field of view of magnetograms that we analyze is $400'' \times 250''$, covering the whole active region of NOAA AR 8100. The noise level in the 1-min cadence data is found to be about 10 G per pixel from a comparison of two successive magnetograms. Detailed procedures for data analysis were well described by Chae (2001) and Chae et al. (2001). During the observations, seven homologous flares stronger than C1 X-ray class occurred in NOAA AR 8100 including two M-class flares. According to Martres et al. (1984), the occurrence of homologous flares can be as frequent as a few events per hour or as infrequent as one in several days. In our case, it is about one event per hour. The flaring locations were identified from the $H\alpha$ flare data of National Geophysical Data Center and a series of $H\alpha$ full disk images of Big Bear

Solar Observatory (BBSO). Basic characteristics of these homologous flares are summarized in Table 1.

Figure 1 shows a temporal variation of magnetic flux for each polarity. The integrated positive and negative magnetic fluxes in the active region are 1.17×10^{22} Mx and -1.46×10^{22} Mx, respectively. It is found from the figure that there was no new magnetic flux emerging during the observing period. The amount of newly emerged flux, if any, should be equal to or less than 3×10^{20} Mx for 6.5 h. There was no noticeable emerging flux for a wider field of view, $800'' \times 800''$.

All the magnetograms were aligned by the non-linear mapping, which takes into account the solar differential rotation effect (Chae 2001; Chae et al. 2001). This procedure is also effective in correcting for the geometrical foreshortening originating from the spherical geometry of the Sun. We have employed a sub-pixel interpolation with a pixel size of $1''$, one half of the original pixel size. To increase the signal-to-noise ratio, we have taken time averages by adopting median values of five successive magnetograms. Since the active region NOAA AR 8100 was located near solar disk center (see Table 1) during the relatively brief period of observations (6.5 hours), the effect of off-center projection is very small, and the line of sight magnetic field is essentially identical to the vertical field. We have determined horizontal velocities by using local correlation tracking method (LCT, November & Simon 1988), which has commonly been used for tracking photospheric intensity patterns such as granulation. For the LCT, there are two important input parameters: FWHM of the apodization window and the time interval between two images for comparison. We select the FWHM of $8''$, four times the spatial sampling size of the MDI full disk data. The time interval for horizontal velocity measurement is set to 20 minutes, which corresponds to about 0.17 pixels when a magnetic flux element moves with a speed of 0.1 km s^{-1} (Chae 2001; Chae et al. 2001). To reduce the contribution of noises, we set to zero the horizontal velocity in the regions with low flux densities (less than 10 G) or low cross-correlation value (less than 0.9).

Vector potential \mathbf{A}_p is determined using a Fourier transform method described in Chae (2001). To minimize the effect of a periodic boundary condition in the computation of \mathbf{A}_p , we employ a 2D computational box of $900'' \times 750''$ size, which is about seven times as large as the region of interest for the present calculation. There were no sizeable magnetic flux concentrations around NOAA AR 8100 that can affect calculations of \mathbf{A}_p . Thus, the boundary effect must be minimal.

3. RESULTS

Figure 2 shows a vector map of vector potential superposed on a MDI longitudinal magnetogram and a BBSO H α image from full-disk data observed on 22:34 UT. As already shown in Chae (2001), the vector potential has a pattern of clockwise rotation in the negative polarity region, and count-clockwise rotation in the positive polarity region. Note that \mathbf{A}_p is the strongest near the polarity inversion line and runs in parallel with the inversion line, which results in a large contribution of photospheric shearing motions near the polarity inversion line to the magnetic helicity increase. The H α image shows two H α brightening associated with the C8.6 flare.

Figure 3 shows the temporal variation of the absolute value of magnetic helicity injection rate with a 5 minute time interval, and the GOES X-ray intensity in 1-8 Å spectral bands. Our estimation of an error of helicity injection rate is made from the standard deviation of the fluctuation during non-flaring time from 24:00 UT to 25:20 UT, which is found to be about $4 \times 10^{40} \text{ Mx}^2 \text{ h}^{-1}$.

The derived magnetic helicity injection rates are predominantly negative throughout the observing period. The sign of magnetic helicity in the active region is inferred to be also negative from Mees Solar Observatory vector magnetograms. Thus the negative sign of helicity injection rate implies accumulation of negative magnetic helicity. For convenience' sake, we deal with the absolute value of magnetic helicity injection rate from now on. The mean helicity injection rate is found to be about $|\langle dH/dt \rangle| = 1.7 \times 10^{41} \text{ Mx}^2 \text{ h}^{-1}$, which is about three times the value Chae et al. (2001) obtained in the filament forming active region NOAA AR 8668. For comparison, we also estimate the contribution of solar differential rotation based on the expression $(dH/dt)_{rot} = \pi F^2 \omega \cos^3 b \sin b / 16$ which was derived by DeVore (2000). Using $\omega = 4.83 \times 10^{-2} \text{ rad day}^{-1}$, $b = -20^\circ$ and $F = 1.17 \times 10^{21} \text{ Mx}$, we obtain $(dH/dt)_{rot} = 1.5 \times 10^{40} \text{ Mx}^2 \text{ h}^{-1}$, which is about one-tenth of $|\langle dH/dt \rangle|$ we obtained. This implies that there do exist photospheric shearing motions which are more important for the magnetic helicity injection than the solar differential rotation, being consistent with the results of Chae (2001) and Chae et al. (2001).

Figure 3 shows that helicity injection rate comprises two kinds of components: a smoothly varying component and spikes. The time variation of the smooth component appears to be correlated with the GOES X-ray flux in Figure 3 to some degree, in that its trough around 24:30 UT coincides with the trough of GOES X-ray flux. On the other hand, two spikes are obviously correlated with the C8.6 and M4.1 flares, respectively. In the first case, the helicity injection rate started to increase at the peak time of the C8.6 flare, and reached its peak about 10 minutes after the X-ray flux peak. The helicity injection rate in the second case evolved almost in phase with the variation of the X-ray flux of the M4.1 flare. In other

flares, there are no spikes in the injection rate that are correlated with flares.

Since the helicity injection rate reflects photospheric motions, we have examined the evolution of horizontal photospheric velocity fields. Figure 4 shows two horizontal flow vector maps taken before and near the flaring time of the M4.1 flare, with a time interval of 30 minutes. The root mean square value of velocity fluctuation is about 0.2 km s^{-1} . We find that there is a persistent pattern in the velocity fields; the positive flux region and the negative flux region move away from each other. Note that this diverging motion has a significant velocity component parallel to the polarity inversion line, indicating that it is essentially a shearing motion. This type of velocity pattern is qualitatively similar to that observed in an emerging active region by Strous et al. (1996). We believe that this lasting pattern of diverging and shearing motion is responsible for the smoothly varying component of the helicity injection rate. The comparison of the two velocity maps in Figure 4 also shows that the major differences between the two maps lie in the encircled localized areas where velocity fields significantly changed. Therefore, the spike in the helicity injection rate can be attributed to these impulsive changes in velocity fields.

The effect of the impulsive and localized changes in velocity fields is best seen in the maps of helicity injection rate density, i.e., the helicity injection rate per unit area $-2(\mathbf{v} \cdot \mathbf{A}_p)B_z$, which are shown in Figure 5. The most noticeable change is the decrease of the positive helicity flux area and the increase of the negative helicity flux area. Two positive kernels (denoted by P1 and P2) disappeared, and four negative kernels (denoted by N1, N2, N3, and N4) either appeared new or were intensified. The four negative helicity kernels exactly match the velocity kernels indicated by the four circles in the lower panel of Figure 4. This finding implies that strong horizontal shear flows localized near the polarity inversion line are mainly responsible for the spike of magnetic helicity injection rate. The helicity fluxes in other velocity kernels seem to be too low to contribute to the helicity injection rate, which is due to either low flux density or weak vector potential.

Now we quantitatively examine the correlation between the magnetic helicity injection by photospheric horizontal motions and the flare energy release in the corona. We denote the i -th flaring time interval as $[t_{i-1}, t_i]$, where t_i is the ending time of X-ray flux emission of the i -th flare. Then we define two integrated quantities: ΔH_i the magnetic helicity accumulated during the flaring time interval and F_i the GOES X-ray flux integrated over flaring time;

$$\Delta H_i = \int_{t_{i-1}}^{t_i} \frac{dH}{dt} dt \quad \text{and} \quad F_i = \int_{t_i-d_i}^{t_i} I_x(t) dt, \quad (3)$$

where I_x is the GOES X-ray intensity in 1-8 Å bands and d_i is the flare duration defined as the time interval between the start and the end of flare X-ray emission. The value of ΔH_i is directly calculated from Figure 3 and the value of F_i for each flare, provided by NOAA, is

tabulated in Table 1. Since the time interval between the C3.9 flare and the M1.3 flare is too short (See Table 1), we consider them as a single event of energy release. The two quantities are plotted in Figure 6. We find a strong positive correlation between the integrated X-ray flux and the amount of helicity deposit by photospheric horizontal motions. Interestingly enough, the X-ray flux increases logarithmically with the helicity deposit.

4. SUMMARY AND DISCUSSION

Using a set of 1 minute cadence full-disk magnetograms taken for 6.5 hours by SOHO/MDI on November 3-4, 1997, we have studied the relationship between solar flares and magnetic helicity change by photospheric shearing motions. First of all, we have found that a series of homologous flares occurred while magnetic helicity was continuously deposited at a significant rate by shear flows in the photosphere. The mean helicity injection rate during the observation is about $\langle dH/dt \rangle = -1.7 \times 10^{41} \text{ Mx}^2 \text{ h}^{-1}$, which is about ten times the contribution from the solar differential rotation. The amount of helicity injected by *shear flows* for 6.5 h is $\Delta H = 1 \times 10^{42} \text{ Mx}^2$. Now let's roughly estimate magnetic helicity that might have been advected by *flux emergence*. Suppose the newly emerged magnetic field lines form a flux rope of one turn twist after emergence. Then the helicity injected by the flux emergence should be equal to the square of the newly emerged flux $(2.5 \times 10^{20} \text{ Mx})^2 = 6 \times 10^{40} \text{ Mx}^2$. This value is much smaller than the helicity injected by shear flows. This finding may be a direct support of a homologous flare model suggested by Choe & Cheng (2000) who showed by numerical simulations that a series of homologous flares take place by continuing shearing motions. This result also comes in parallel with Chae et al. (2001)'s finding that formation of a prominence is associated with magnetic helicity injection by shear flows, which supports Choe & Lee (1992)'s work on the prominence formation.

It would be interesting to compare our results with other recent studies. Demoulin et al. (2002a) studied possible sources of the magnetic helicity injection into the solar corona and then concluded that *differential rotation* is not efficient enough for supplying the magnetic helicity of active regions and coronal mass ejections (CMEs). Demoulin et al. (2002b) further argued that photospheric shearing motions are relatively inefficient to bring magnetic helicity into the corona compared to the helicity carried by significantly twisted flux tubes. On this basis, they suggested that the contribution by emerging fluxes (first term of Equation 1) may be more important than that by photospheric horizontal motions (second term). Based on our results, we agree with Demoulin et al. (2002a,b) conclusion that differential rotation is not efficient. But we think it is hasty to exclude all kinds of photospheric shearing motions from the list of possible sources of the magnetic helicity injection. As a matter of fact, our

results indicate that there do exist photospheric shear flows that can inject significant amount of magnetic helicity into the solar corona. Demoulin et al.’s suggestion that the advection term are more important as a helicity source might be true, but the argument were not based on direct estimations of the two terms. More recently, Kusano et al. (2002) developed a way to derive directly both terms of equation (1) and applied it to NOAA AR 8100 from November 1 to 5, 1997. This active region is the same active region that we analyze. They determined vertical velocity components from the induction equation by solving an inversion problem, and used interpolated magnetic vector field data to fill up night time gaps. They showed that the two terms were comparable to each other with mainly opposite signs. They also found that there is a certain correlation between magnetic helicity injection and GOES X-ray activity. Then they argued that horizontal shear motions are important for some type of flares and emerging fluxes for other types of flares (K. Kusano, private communication). We agree with their opinion that the relative importance between the two terms may depend on the evolution of an active region.

From our study we also found that the helicity injection rate impulsively increased and then decreased around the times of two major (M4.2 and C8.1) flares. These spiky helicity injection rates are attributed to strong transient shearing motions localized near the polarity inversion line. This result implies that magnetic helicity in the corona increased rapidly around the flaring times, although some helicity may be lost to interplanetary space through coronal mass ejection or plasmoid ejection. We are investigating several other cases for a further study, and the preliminary results suggest that the abrupt change of magnetic helicity rate often occurs during strong flares. Harvey & Harvey (1976) analyzed magnetograms and Dopplergrams in the $H\alpha$ and Fe I 6569 Å lines of MacMath region 10385 in which 14 flares took place during their observations. From this study, they found strong, oppositely moving photospheric Doppler velocity structures associated with solar flares, particularly as the active region approaches to the limb. Then they argued that horizontal photospheric motions play a crucial role in producing flares by twisting and shearing magnetic fields.

Finally, we have found a strong positive correlation between the helicity accumulated by photospheric horizontal motions during the flaring time interval and the integrated X-ray flux of the subsequent flare. The X-ray flux increases logarithmically with the helicity accumulation. This indicates that the occurrence of a series of homologous flares in an active region is physically related to the accumulation of magnetic helicity in the corona by photospheric shearing motions. We can roughly estimate the magnetic energy deposit associated with the helicity injection during a flaring time interval as

$$\Delta E \sim \frac{\Delta H}{L} \sim 10^{31} \text{erg}, \quad (4)$$

where L is the characteristic length of magnetic loops in an active region taken to be 10^5

km. This value is comparable to the energy of a typical solar flare.

Our results raise intriguing questions on physics of flares. Previous studies on the flaring time interval (waiting time) and the corresponding GOES X-ray fluxes of flares (Wheatland 2000; Moon et al. 2001) showed that there is no clear correlation between the waiting time and the corresponding flare X-ray flux. This result was regarded to support the self-organized criticality (SOC) model of the solar corona because in a self-organized critical state the size of any output incidence is independent of the driving mode (Bak 1996). According to our results, however, solar flares seem to take place in immediate response to an abrupt increase of helicity injection rate (see Figure 2). Also, the strong positive correlation between the flare X-ray flux and the accumulated helicity casts some skepticism on the SOC picture.

However, our results do not show an unanimous favor for other paradigms of flare mechanisms either. It is also not clear from our results whether the condition for flare onset is to reach a critical state characterized by a certain amount of magnetic helicity (or magnetic shear) (Kusano, Suzuki, & Nishikawa 1995; Choe & Lee 1996), or to have an external driver impulsive enough to disturb a linearly stable system or strong enough to power the flaring system synchronously (e.g., Kan et al. 1983). Since each piece of our results seems to more or less favor different mechanisms, a further extensive study is required to answer these questions.

In some flares we have studied, the maximum of helicity injection rate is reached a little while after the maximum of X-ray intensity. The most conspicuous example is the C8.6 flare (see Figure 3). In general, magnetic reconnection in a bipolar field reduces the magnetic shear observed in the photosphere. However, if a shearing motion is extremely active during a flare as in the above case, the magnetic shear in the photosphere may be increased after a flare. This may explain the observation by Wang et al. (1994) that magnetic shear indeed increased after some X-ray flares.

We are thankful to the BBSO observing staff for their support in obtaining the data. We appreciate Dr. Kusano and an anonymous referee for their valuable comments, which helped us in improving the present paper. This work has been supported by NASA grants NAG5-10894 and NAG5-7837, by MURI grant of AFOSR, by the US-Korea Cooperative Science Program (NSF INT-98-16267), by NRL M10104000059-01J000002500 of Korean government, and by the BK 21 project of the Korean government. G. S. C. has been supported by the DoE Contract DE-AC02-76-CHO3073 and the NSF grant ATM-9906142. SOHO is a project of international cooperation between ESA and NASA.

REFERENCES

- Bak, P. 1996, *How Nature Works: the Science of Self-Organized Criticality* (New York: Copernicus)
- Berger, M. A. 1999, in *Magnetic Helicity in Space and Laboratory Plasmas*, ed. M. R. Brown, R. C. Canfield, & A. A. Pevtsov (Geophys. Monogr. 111; Washington, DC: AGU), 1
- Berger, M. A., & Field, G. B. 1984, *J. Fluid Mech.*, 147, 133
- Burlaga, L. F. 1988, *J. Geophys. Res.*, 93, 7217
- Canfield, R. C., & Pevtsov, A. A. 1999, in *Magnetic Helicity in Space and Laboratory Plasmas*, ed. M. R. Brown, R. C. Canfield, & A. A. Pevtsov (Geophys. Monogr. 111; Washington, DC: AGU), 197
- Chae, J. 2000, *ApJ*, 540, L115
- Chae, J. 2001, *ApJ*, 560, L95
- Chae, J., Wang, H., Qiu, J., Goode, P. R., Strous, L., & Yun, H. S. 2001, *ApJ*, 560, 476
- Choe, G. S. & Lee, L. C. 1992, *Sol. Phys.*, 138, 291
- Choe, G. S. & Lee, L. C. 1996, *ApJ*, 472, 372
- Choe, G. S. & Cheng, C. Z. 2000, *ApJ*, 541, 449
- Demoulin, P., Mandrini, C. H., van Driel-Gesztelyi, L., Thompson, B. J., Plunkett, S., Kovari, Zs., Aulanier, G., & Young, A. 2002, *A&A*, 382, 650
- Demoulin, P., Mandrini, C. H., van Driel-Gesztelyi, L., Lopez Fuentes, M. C., & Aulanier, G. 2002, *Sol. Phys.*, in press
- DeVore, C. R. 2000, *ApJ*, 539, 944
- Hagyard, M. J. & Pevtsov, A. A. 1999, *Sol. Phys.*, 189, 25
- Harvey, K. L. & Harvey, J. W. 1976, *Sol. Phys.*, 233, 246
- Kan, J. R., Akasofu, S.-I., & Lee, L. C. 1983, *Sol. Phys.*, 84, 153
- Kusano, K., Suzuki, Y., & Nishikawa, K. 1995, *ApJ*, 441, 942
- Kusano, K., Maeshiro, T., Yokoyama, T., & Sakurai, T. 2002, in *Yohkoh 10 meeting* (<http://solar.physics.montana.edu/Y10/abstracts.html>)

- Martres, M.-J., Woodgate, B. E., Mein, N., Mouradian, Z., Rayrole, J., Schmieder, B., Simon, G., & Soru-Escout, I. 1984, *Adv. Space Research*, 4, No.7, 5
- Moon, Y.-J., Choe, G. S., Yun, H. S., & Park, Y. D. 2001, *J. Geophys. Res.*, 106, A12, 29951
- November, L. J., & Simon, G. W. 1988, *ApJ*, 333, 427
- Pevtsov, A. A., & Canfield, R. C. 1999, in *Magnetic Helicity in Space and Laboratory Plasmas*, ed. M. R. Brown, R. C. Canfield, & A. A. Pevtsov (*Geophys. Monogr.* 111; Washington, DC: AGU), 103
- Ranns, N. D. R., Harra, L. K., Matthews, S. A., & Culhane, J. L. 2000, *A&A*, 360, 1163
- Rust, D. M. 1999, in *Magnetic Helicity in Space and Laboratory Plasmas*, ed. M. R. Brown, R. C. Canfield, & A. A. Pevtsov (*Geophys. Monogr.* 111; Washington, DC: AGU), 221
- Scherrer, P. H., et al. 1995, *Sol. Phys.*, 162, 129
- Strous, L. H., Scharmer, G., Tarbell, T. D., Title, A. M., & Zwaan, C. 1996, *A&A*, 306, 947
- Wang, H., Ewell, M. W., Jr., Zirin, H., Ai, G. 1994, *ApJ*, 424, 436
- Wheatland, M. S. 2000, *Sol. Phys.*, 191, 381
- Woodgate, B. E., Martres, M.-J., Smith, J. B., Jr., Stron, K. T., McCabe, M. K., Machado, M. E., Gaizauskas, V. Stewart, R. T., & Sturrock, P. A. 1984, *Adv. Space Res.*, 4(7), 11

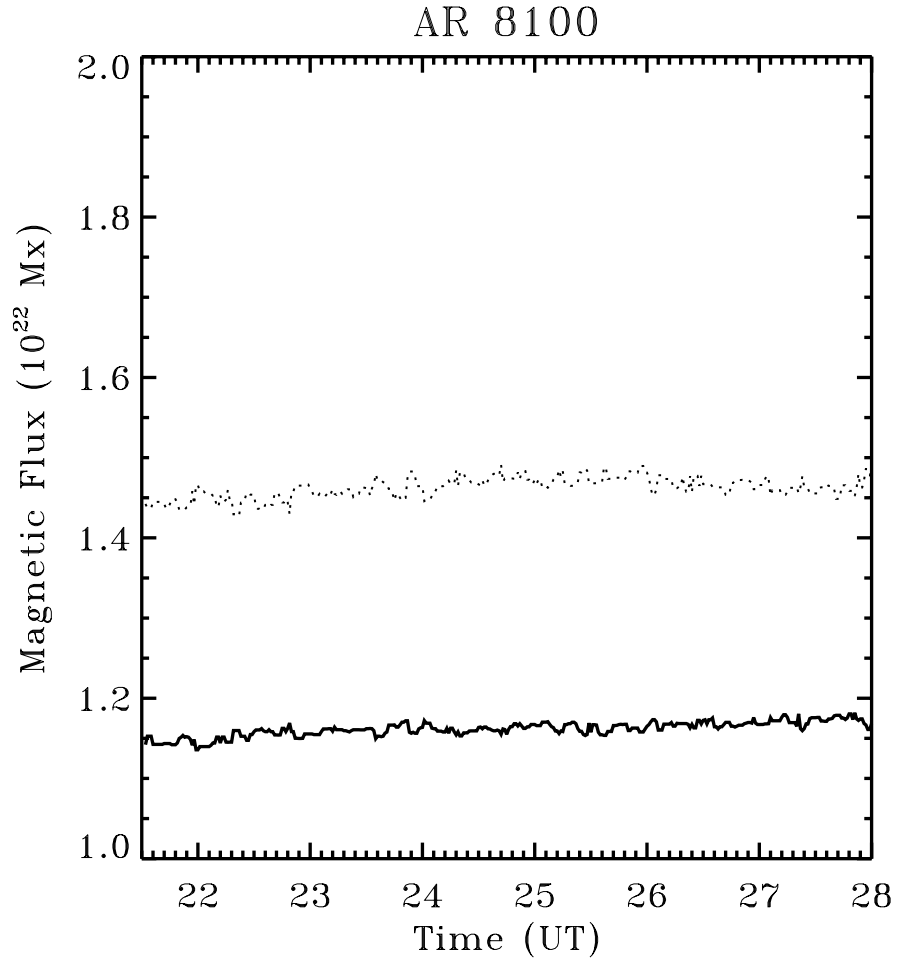


Fig. 1.— Temporal magnetic flux variation for each polarity in NOAA AR 8100. Solid line indicates positive polarity and dotted line, negative polarity.

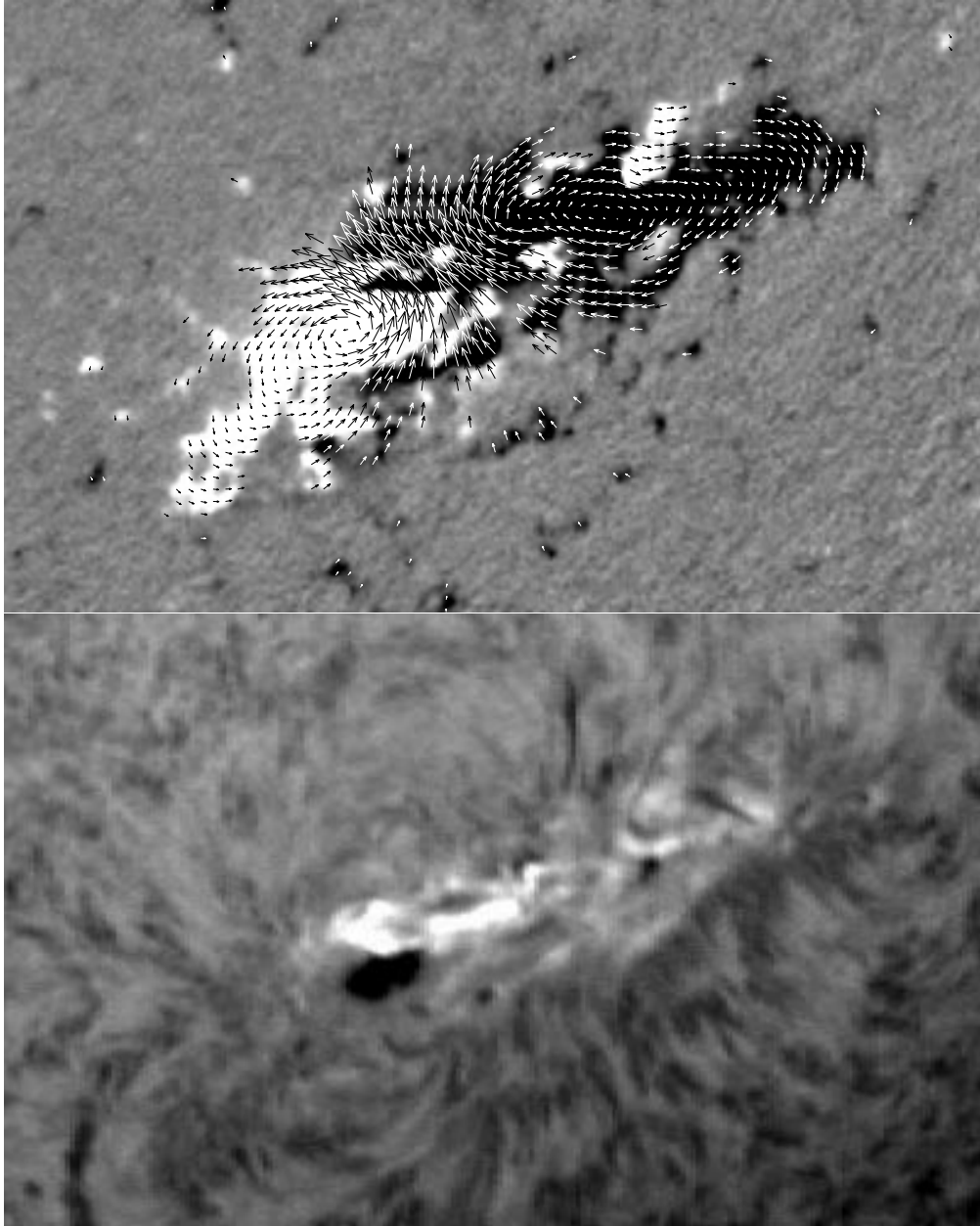


Fig. 2.— \mathbf{A}_p vectors (upper panel) calculated from a MDI longitudinal magnetogram of NOAA AR 8100 and a BBSO $H\alpha$ image (lower panel) observed at 22:34 UT.

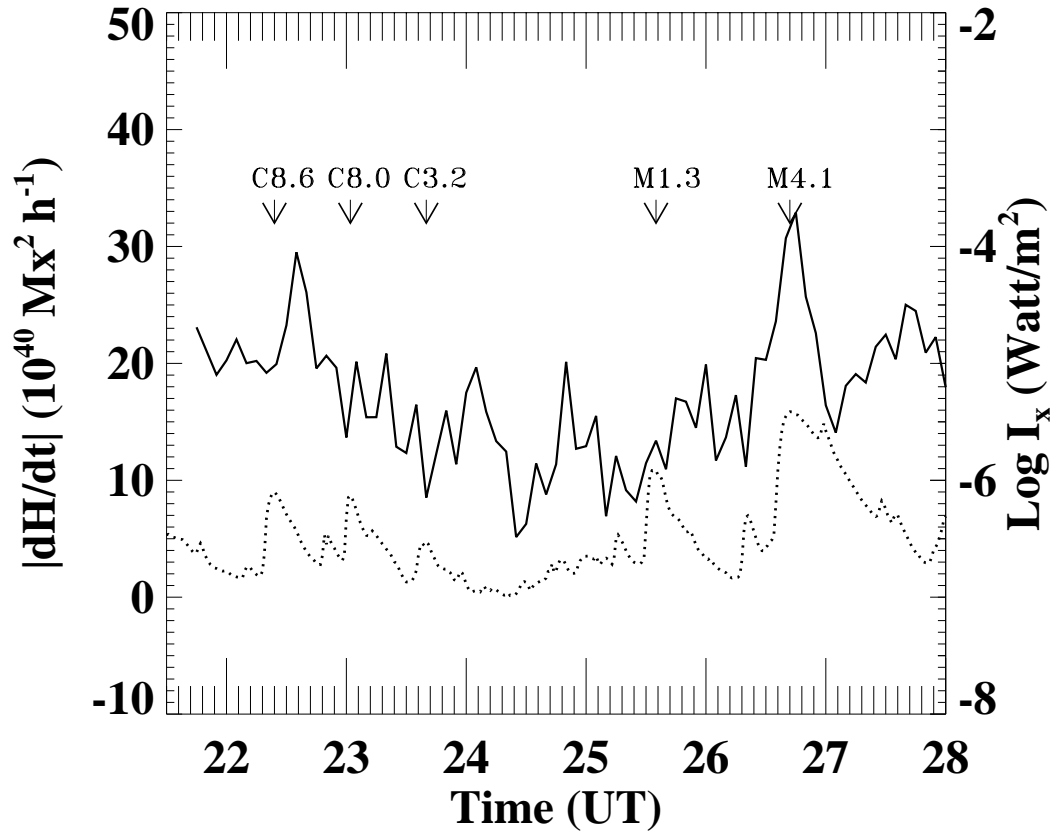


Fig. 3.— Temporal evolution of the magnetic helicity rate (solid line) by horizontal photospheric motions and the GOES intensity (dotted line) in 1-8 Å bands. The GOES intensity is referenced to the right vertical axis and the arrows indicate the X-ray intensity peak of homologous flares.

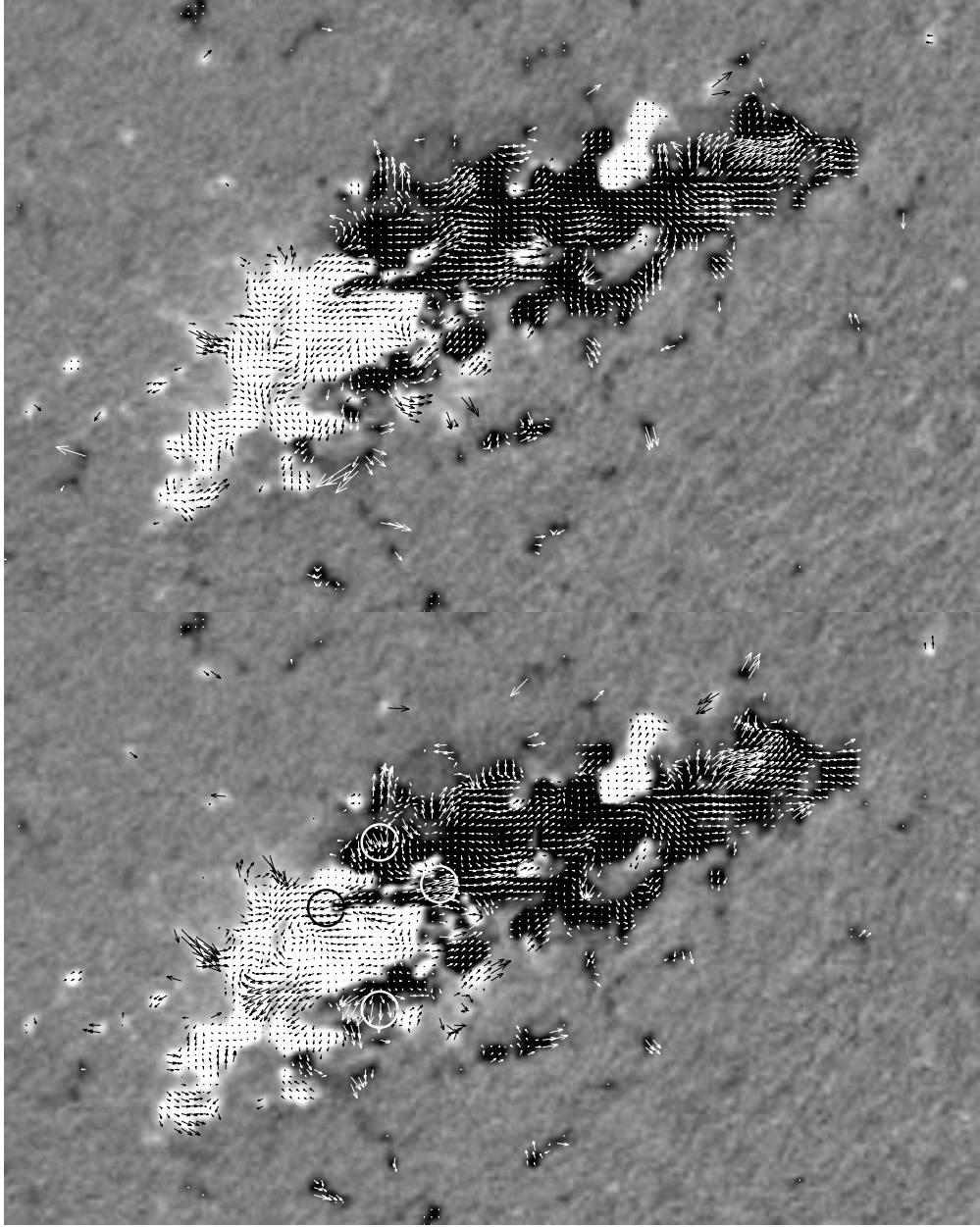


Fig. 4.— Vector maps of photospheric horizontal flows superposed on MDI magnetograms. The upper panel was taken at 02:15 UT and the lower panel taken at 02:45 UT, near the peak time of the M4.5 flare. In the lower panel, the largest arrow corresponds to 1.2 km s^{-1} .

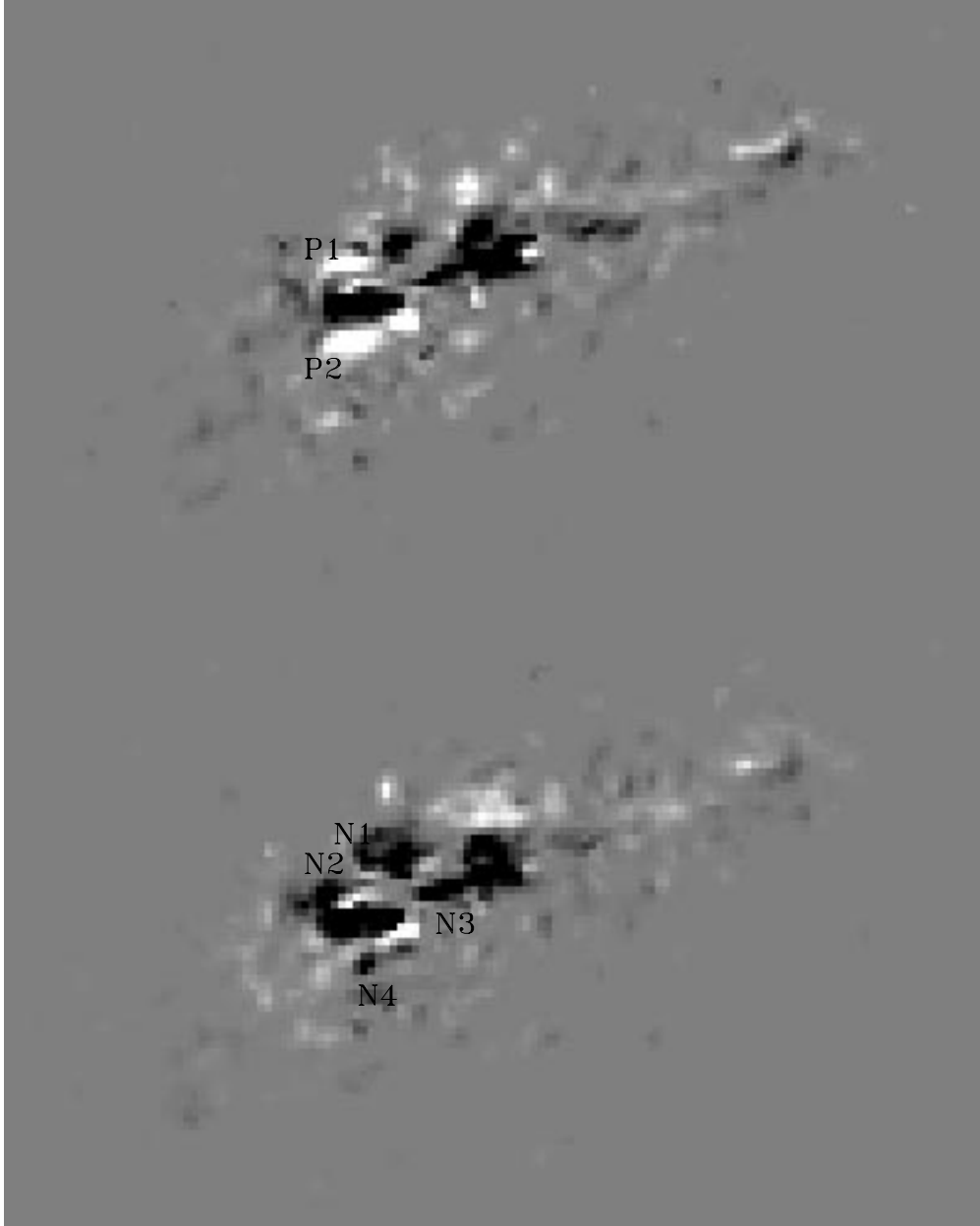


Fig. 5.— Maps of helicity injection rate density, i.e., $-2(\mathbf{v} \cdot \mathbf{A}_p)B_z$. The upper panel was taken at 02:15 UT and the lower panel taken at 02:45 UT, near the peak time of the M4.5 flare.

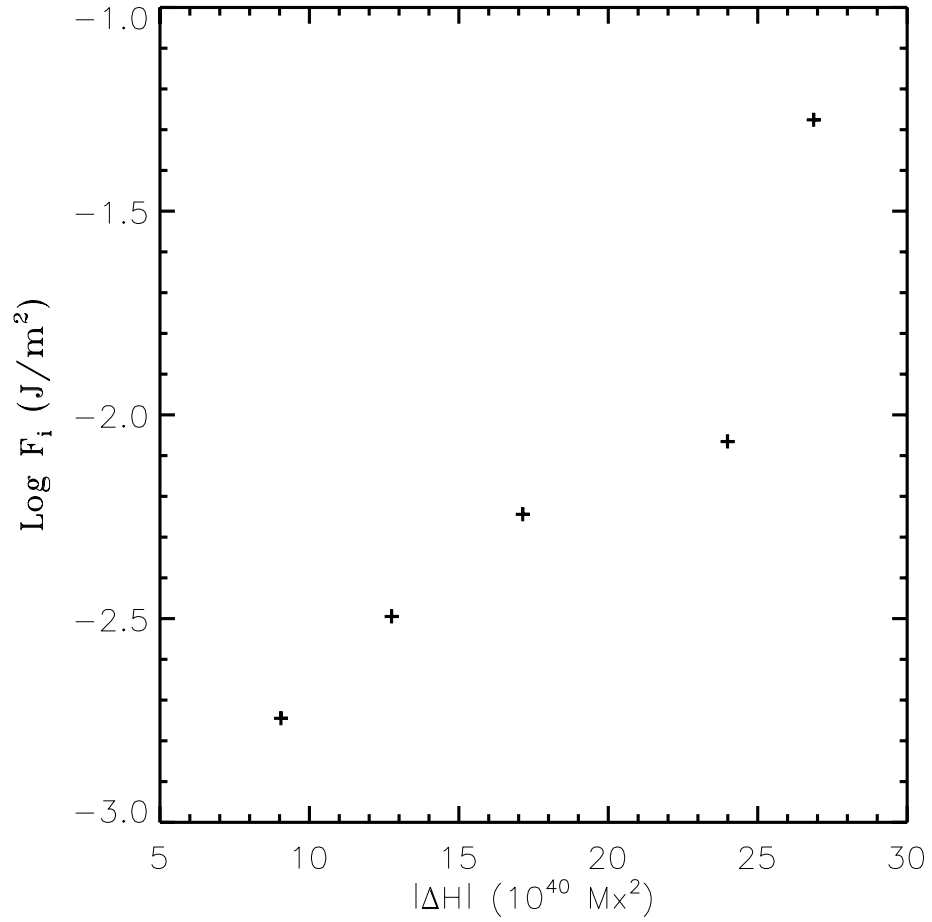


Fig. 6.— Absolute value of the magnetic helicity induced by photospheric horizontal motions accumulated during the flaring time interval vs the corresponding GOES X-ray flux integrated over the flaring time.

Table 1. Basic observational parameters of homologous flares that occurred in NOAA AR 8100. F_i is the X-ray flux integrated over the flaring time.

Date	Start	Peak	End	Coord.	X-ray Class	$F_i(J/m^2)$
97/11/3	21:20	21:25	21:42	S19W22	C3.9	4.5E-3
97/11/3	22:16	22:24	22:32	S19W23	C8.6	5.7E-3
97/11/3	22:58	23:02	23:07	S20W23	C8.0	3.2E-3
97/11/3	23:33	23:40	23:44	S20W23	C3.2	1.8E-3
97/11/4	01:13	01:16	01:20	S20W24	C3.9	4.5E-3
97/11/4	01:27	01:35	01:40	S20W24	M1.3	7.3E-3
97/11/4	02:32	02:42	03:03	S20W24	M4.1	5.3E-2